

Article

Optimization of Discontinuous Polymer Flooding Processes for Offshore Oilfields Using a Novel PSO–ICA Algorithm

Engao Tang^{1,2}, Jian Zhang^{1,2}, Yi Jin^{1,2}, Lezhong Li^{1,2}, Anlong Xia³, Bo Zhu³ and Xiaofei Sun^{3,*} 

¹ State Key Laboratory of Offshore Oil & Gas Exploitation, Beijing 100028, China; tangeg@cnooc.com.cn (E.T.); zhangjian@cnooc.com.cn (J.Z.); jinyi6@cnooc.com.cn (Y.J.); lilzh3@cnooc.com.cn (L.L.)

² CNOOC Research Institute Limited, Beijing 100028, China

³ School of Petroleum Engineering, China University of Petroleum (East China), Qingdao 266580, China; 1802010622@s.upc.edu.cn (A.X.); 2102010127@s.upc.edu.cn (B.Z.)

* Correspondence: xfsun@upc.edu.cn; Tel.: +86-130-2167-8278

Abstract: Recently, discontinuous polymer flooding has been proposed and successfully applied in some offshore oilfields. The performance of discontinuous polymer flooding depends on various operational parameters, such as injection timing, polymer concentrations, and crosslinker concentrations of four types of chemical slugs. Because the number of the operational parameters are large and they are nonlinearly related, the traditional reservoir numerical simulation might not simultaneously obtain the optimal results of these operational parameters. In this study, to simulate the discontinuous polymer flooding processes, a simulation model was built using a commercial reservoir simulator (CMG STARS), in which the mechanisms of the four types of chemical slugs were considered, such as polymer viscosification, adsorption, and degradation. Then, a PSO–ICA algorithm was developed by using the PSO algorithm to improve the exploration ability of the ICA algorithm. The codes were written with MATLAB and linked to CMG STARS to perform optimization processes. Finally, the PSO–ICA algorithm was compared with the ICA and PSO algorithms on benchmark functions to verify its reliability and applied to optimize a discontinuous polymer flooding process in a typical offshore oilfield in Bohai Bay, China. The results showed that the developed PSO–ICA algorithm had lower iteration numbers, higher optimization accuracy, and faster convergence rate than these of PSO and ICA, indicating that it was an effective method for optimizing the operational parameters of discontinuous polymer flooding processes. Compared to the continuous polymer flooding, the discontinuous polymer flooding had a higher oil production rate, a lower water cut, and a lower residual oil saturation. The net present value of the optimal scheme of discontinuous polymer flooding reached 7.49×10^8 \$, which is an increase of 6% over that of the scheme of continuous polymer flooding. More research including selecting more reasonable parameters of the PSO–ICA algorithm to increase its optimization accuracy and convergence rate, comparing with other available optimization algorithms, and verifying the performance of the optimal scheme of discontinuous polymer flooding in the practical offshore oilfield will be required in the future.

Keywords: discontinuous polymer flooding; optimization algorithm; imperialist competitive algorithm; particle swarm optimization; offshore oilfields; reservoir simulation; gel; polymer



Citation: Tang, E.; Zhang, J.; Jin, Y.; Li, L.; Xia, A.; Zhu, B.; Sun, X.

Optimization of Discontinuous Polymer Flooding Processes for Offshore Oilfields Using a Novel PSO–ICA Algorithm. *Energies* **2024**, *17*, 1971. <https://doi.org/10.3390/en17081971>

Academic Editors: Riyaz Kharrat and Hossein Hamidi

Received: 25 February 2024

Revised: 24 March 2024

Accepted: 8 April 2024

Published: 21 April 2024



Copyright: © 2024 by the authors. Licensee MDPI, Basel, Switzerland. This article is an open access article distributed under the terms and conditions of the Creative Commons Attribution (CC BY) license (<https://creativecommons.org/licenses/by/4.0/>).

1. Introduction

Polymer flooding is a promising enhanced oil recovery method to increase oil recovery [1]. The addition of soluble polymer leads to an increase in the viscosity of injection water, a decrease in water mobility, and an increase in sweep efficiency [2]. In addition, polymer viscoelastic behavior also improves micro displacement efficiency [3–5]. Because the facilities required to implement polymer flooding meet the space and weighing requirements of offshore platforms, polymer flooding is gradually being applied in offshore oilfields [6]. For example, an offshore polymer flooding in the Dos Cuadras field near Santa

Barbara, California was implemented in 1986 [7]. In addition, a polymer flooding was carried out in Bohai oilfield, China, from 2008 to 2016. The cumulative oil production of nine wells reached $10.80 \times 10^4 \text{ m}^3$ [8]. However, offshore oilfields with high heterogeneity present higher-permeability zones through which the injected polymer solution flows from the injector to the producer, resulting in high water cut [9]. In addition, the continuous injection of polymer solution commonly results in high injection pressure, reduced polymer injection, and increased application cost.

Chemical materials, such as gels, crosslinked particles gels, and crosslinked polymer microspheres, are often injected into the reservoirs to preferentially seal the higher-permeability zones [10–16]. In addition, Claridge (1978) proposed that a polymer solution can be injected using several slugs with gradually decreased polymer concentrations, reducing the polymer loading and viscous fingering compared to one polymer slug [17]. Most reported projects worldwide have followed this scheme [18,19]. Recently, a new chemical flooding method called discontinuous polymer flooding has been proposed to deal with the aforementioned problems of polymer flooding and applied in mature offshore oilfields. For instance, after 5 months of discontinuous polymer flooding in the B reservoir in Bohai Bay, China, the average oil production rate increased by 115% and the water cut decreased by 15% compared with the continuous polymer flooding [20]. In this method, four types of chemical slugs (anti-dilution gel slug, polymer slug, long-acting gel slug, and polymer slug with low concentrations) were injected into the reservoir to improve the performance of polymer flooding. First, an anti-dilution gel slug was injected to seal the higher-permeability zones. Then, a polymer slug was injected to displace the oil. When the water cut or injection pressure sharply increased during the injection of the polymer slug, a long-acting gel slug or a polymer slug with a low concentration was injected to improve the sweep efficiency of polymer or decrease the injection pressure.

The performance of discontinuous polymer flooding depends on various operational parameters of the four types of chemical slugs, such as injection timing, polymer concentrations, and crosslinker concentrations. The number of the operational parameters are large and they are nonlinearly related. Using reservoir numerical simulation to optimize the operational parameters is time-consuming and expensive, meaning it might not simultaneously obtain the optimal results of these operational parameters.

Recently, optimization algorithms have been used to deal with the complex optimization problems [21–24]. Compared with reservoir numerical simulation, optimization algorithms are more efficient and can save optimization time. Specially, Sayyafzadeh and Keshavarz determined the optimal gas composition and gas injection rate for a coal-bed methane reservoir by using a genetic algorithm (GA) [25]. Eshraghi et al. optimized the operational parameters of a miscible CO₂ injection process using particle swarm optimization (PSO) and GA. They found that PSO exhibited better performance than GA [26]. Ghadami et al. optimized a chemical flooding process by using response surface methodology and PSO to maximize the oil recovery. They found that PSO is a better algorithm for the optimization of chemical flooding processes [27]. Al Dossary and Nasrabadi obtained the optimal well locations using the imperialist competitive algorithm (ICA). The results showed that ICA obtained the optimal well location faster than GA and PSO, and also achieved a higher net present value [28].

Aside from the oil industry, ICA also shows a good performance for optimization in other domains, such as electrical power system optimization [29,30], neural network training [31], flow shop scheduling [32], data clustering [33], facility layout problem [34], minimal spanning tree problem [35], and so on. Though the ICA has some advantages such as a fast convergence speed and better optimized results, the exploration capability of ICA is unsatisfactory. Several modified methods have been proposed to solve the aforementioned problem. For instance, Bahrami and Abdechiri introduced a chaotic map to adjust the angles of colonies' movements toward imperialists [36,37]. Abdechiri proposed an adaptive ICA in which an absorption policy was used to change the angles of colonies

moving towards imperialists [38]. Khaled developed a fuzzy adaptive ICA where the deviation parameter was adaptively adjusted using a fuzzy controller [39].

In this study, 120 operational parameters (injection timing, polymer concentrations, and crosslinker concentrations of four types of chemical slugs for 12 injection wells) were simultaneously optimized to find the optimal net present value (NPV) of a discontinuous polymer flooding process. First, to simulate the discontinuous polymer flooding processes, a simulation model was built using a commercial reservoir simulator (CMG STARS), in which the mechanisms of the four types of chemical slugs were considered, such as polymer viscosification, adsorption, and degradation. Then, a PSO–ICA algorithm was developed by using the PSO algorithm to improve the exploration ability of ICA algorithm. The codes were written in MATLAB and linked to CMG STARS to perform optimization processes. Finally, the PSO–ICA algorithm was compared with the ICA and PSO algorithms on benchmark functions to verify its reliability and applied to optimize a discontinuous polymer flooding process in a typical offshore oilfield in Bohai Bay, China. To the best of our knowledge, there are no reservoir numerical simulations and optimizations conducted to investigate discontinuous polymer flooding processes. This study provides an effective method to conduct the optimal design of discontinuous chemical flooding and can be used as a reference in practical applications of the discontinuous polymer flooding process for enhancing oil recovery in offshore oilfields.

2. Reservoir Simulation Model

To represent a typical offshore oilfield at Bohai Bay, China, a reservoir model was developed with dimensions of 4200 m × 1800 m × 320 m in x, y, and z directions, respectively, and was discretized into 86 × 44 × 174 cells (total 658,416 cells) (Figure 1). A total of 12 injection wells and 28 production wells were drilled with a well spacing of 190 m. To simulate the discontinuous polymer flooding processes, a simulation model was built using a commercial reservoir simulator (CMG STARS). The model contains nine components (water, crosslinker 1, polymer 1, crosslinker 2, polymer 2, anti-dilution gel and long-acting gel, oil, and solution gas), which appear in oleic phase, gaseous phase, and aqueous phase. Considering the different physical and chemical properties of the anti-dilution gel and long-acting gel, two chemical reaction formula were used to describe the formation of the anti-dilution gel and long-acting gel.



where a , b , c , d , e , and f are the chemical reaction coefficients, which are determined by matching the core displacement experiments.

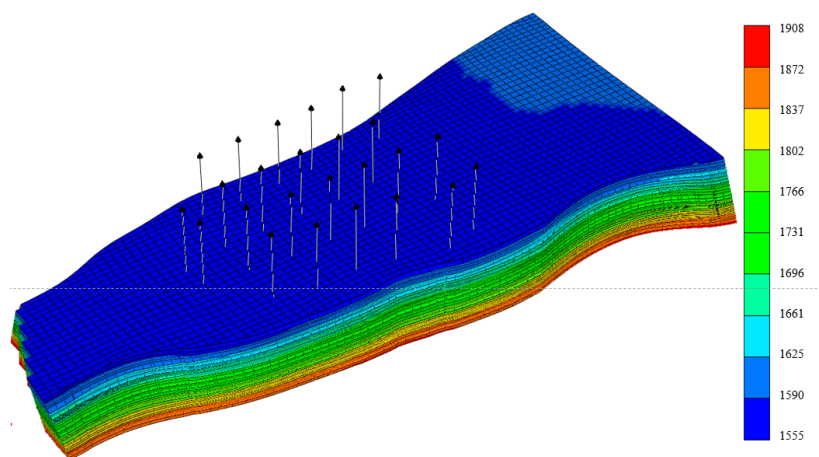


Figure 1. Three-dimensional reservoir model of the typical offshore oilfield.

To characterize the effects of the four types of chemical slugs on discontinuous polymer flooding, the following mechanisms were considered in the simulation model.

(1) The effects of shear rate on polymer viscosity

The effects of shear rate on polymer viscosity is modeled by using Meter's equation [40]:

$$\mu_p = \mu_w + \frac{\mu_p^0 - \mu_w}{1 + \left(\frac{\dot{\gamma}}{\dot{\gamma}_{1/2}}\right)^{p_\alpha - 1}} \quad (3)$$

where $\dot{\gamma}$ is the shear rate, s^{-1} ; μ_p^0 and μ_w are the polymer and water viscosity, $mPa \cdot s$; $\dot{\gamma}_{1/2}$ is the shear rate when the viscosity is the average value of μ_p^0 and μ_w , s^{-1} ; p_α is an empirical coefficient.

(2) The adsorption of polymers and gels

During the discontinuous polymer flooding processes, some of the polymers and gel will adsorb on the surface of rocks. The adsorption strength is mainly related to the polymer and gel type, saturations, and rock type [40]. The following equation is used to characterize the adsorption phenomenon.

$$Ad_S = Ad_L \times \frac{\rho_r \times (1 - \phi)}{\phi} \times C_f \quad (4)$$

where Ad_S is the adsorption capacity of polymer or gel in the model, $gmol/m^3$; Ad_L is the static adsorption capacity of polymer or gels measured in the laboratory, $\mu g/g$; ρ_r is the rock density of the reservoir, g/cm^3 ; ϕ is the porosity, %; C_f is a factor for unit conversion between the model and laboratory.

(3) The permeability reduction

The adsorption of polymer on the surface of rocks reduces the permeability. The aforementioned phenomenon is characterized by the permeability reduction factor, modeled as follows:

$$K = \frac{k}{R_k} \quad (5)$$

where k and K are the absolute permeability of rock before and after polymer flooding, μm^2 ; R_k is the permeability reduction factor, which is a function of the polymer adsorption and residual resistance factor.

$$R_k = 1 + (RRF - 1) \times \frac{AD}{AD_{MAX}} \quad (6)$$

where RRF is the residual resistance factor; AD is the cumulative adsorption capacity of the polymer or gel per unit volume of rock, $gmole$; AD_{MAX} is the maximum adsorption capacity of polymer or gel per unit volume of rock, $gmole/m^3$.

(4) Inaccessible pore volume

The pore volume in the rock that the polymer solution cannot enter due to the large polymer structure can be calculated as follows:

$$\phi_p = IPV \times \phi \quad (7)$$

where ϕ_p is the porosity value of the reservoir pores that the polymer solution cannot enter, %; IPV is the inaccessible pore volume, %, which is measured by experiments.

(5) Polymer degradation

During polymer flooding processes, physical, chemical, and biological reactions commonly occur in the formation, resulting in polymer degradation. The following equations are used to characterize the polymer degradation phenomena.

$$g\text{Polymer} \rightarrow h\text{Water} \quad (8)$$

$$rrf = \frac{\ln 2}{T_{1/2}} \quad (9)$$

where g and h are the chemical reaction coefficients; rrf is the reaction rate, 1/ day; $T_{1/2}$ is the half-life of the polymer solution, days.

(6) Polymer and gel viscosification

Compared with water flooding, discontinuous polymer flooding has higher sweep efficiency because the polymer and gel can increase the viscosity of the injection water. The aforementioned mechanism is depicted as follows [41].

$$\ln(\mu_\alpha) = \sum_{i=1}^n f(x_{ai}) \ln(\mu_{ai}) \quad (10)$$

where μ_a and μ_{ai} are the viscosity of the aqueous phase and the viscosity of component i in the aqueous phase, respectively, mPa·s; n is the component number; x_{ai} is the molar fraction of the component i in the aqueous phase; $f(x_{ai})$ is a coefficient of the component i in the aqueous phase. Table 1 and Figure 2 show the detailed fluid and reservoir parameters used in the reservoir simulation model.

Table 1. The detailed fluid and reservoir parameters.

Reservoir Properties	Values
Average depth (m)	1731.74
Average reservoir porosity (%)	16.1
Average reservoir permeability (mD)	440.7
Reservoir pressure (kPa)	101
Reservoir temperature (°C)	70
Rock compressibility (1/kPa)	10 ⁻⁴
Average oil saturation (%)	56
Fluid properties	Values
Oil density (kg/m ³)	838
Oil viscosity (mPa·s)	1.9478
Residual resistance factor	1.3
Inaccessible pore volume	0.3
ADMAXT of polymer (gmole/m ³)	6.26
ADMAXT of anti-dilution gel (gmole/m ³)	8.25
ADMAXT of long-acting gel (gmole/m ³)	6.60
The half-life of the polymer solution (day)	1040
Results of the polymer adsorption experiment	
Mole fraction of polymer (%)	Adsorption capacity (gmole/m ³)
0	0
0.0005	5.43
0.001	5.94
0.0015	6.18
0.002	6.25

Table 1. Cont.

Results of the anti-dilution gel adsorption experiment	
Mole fraction of Anti-dilution gel (%)	Adsorption capacity (gmole/m ³)
0	0
0.0005	7.43
0.001	7.94
0.0015	8.18
0.002	8.25
Results of the long-acting gel adsorption experiment	
Mole fraction of Long-acting gel (%)	Adsorption capacity (gmole/m ³)
0	0
0.0005	5.94
0.001	6.35
0.0015	6.54
0.002	6.60

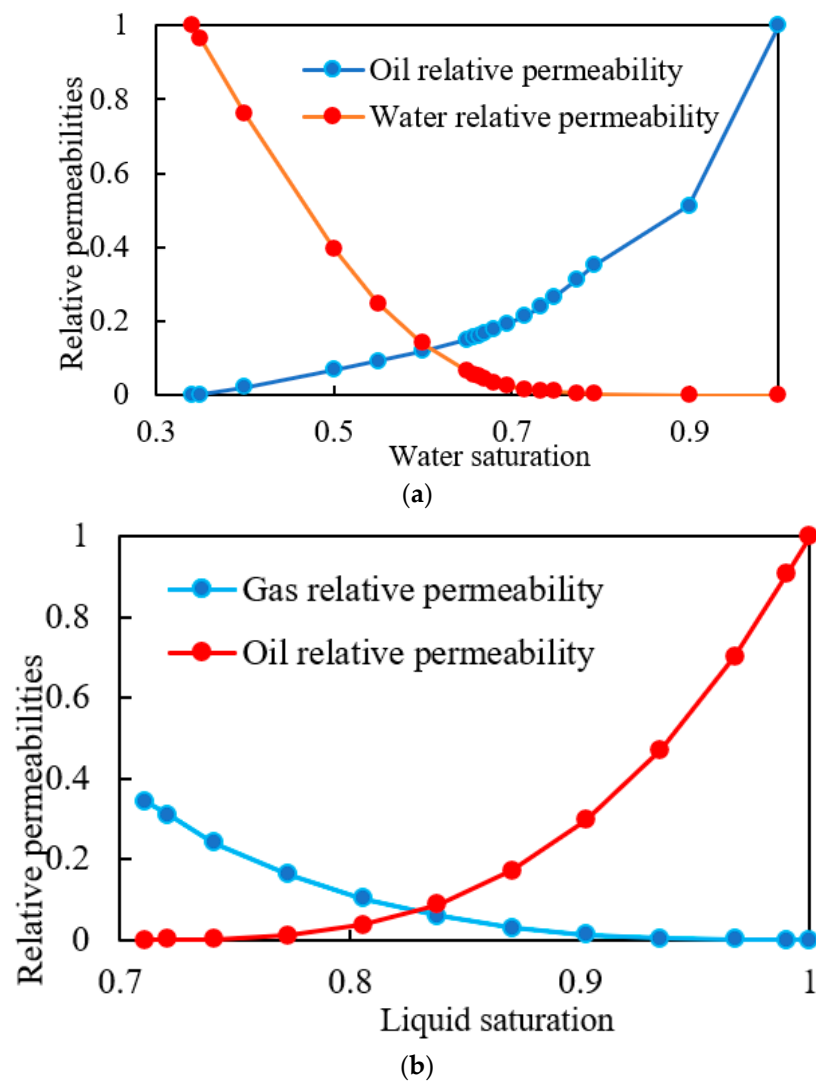


Figure 2. The relative permeabilities of (a) oil-water and (b) gas-fluid.

From 2006 to 2022, water flooding was used to develop the offshore oilfield. The cumulative oil production was 4×10^6 m³ and the cumulative injection volume of 12 injection wells was 2.02×10^7 m³, respectively. The production model was developed by

inputting the production and injection data into CMG STARS. After the aforementioned process, a complete simulation model for discontinuous polymer flooding was developed, which laid a foundation for subsequent optimization processes.

3. Methodology

3.1. Objective Function

In this study, the objective function optimized by the developed PSO–ICA algorithm was the net present value, which was calculated by the following equation [42]:

$$NPV = \sum_{t=1}^T \frac{R_t}{(1+i)^t} \quad (11)$$

$$R_t = Benefits - Costs \quad (12)$$

where NPV is the net present value, 10^8 \$; R_t is the net cash inflow (*Benefits*) minus cash outflow (*Costs*) during a period of time (t), 10^8 \$; i is a discount rate; T is the operation time of a discontinuous polymer flooding process, year. The *Benefits* and *Costs* of the discontinuous polymer flooding process are calculated by the following equations:

$$Benefits = (Q_{oil}^d - Q_{oil}^c) \times P_{oil} \quad (13)$$

$$Costs = (P_{ag}^c \times M_{ag}^c) + (P_{ag}^p \times M_{ag}^p) + (P_p \times M_p) + (P_{lg}^c \times M_{lg}^c) + (P_{lg}^p \times M_{lg}^p) \quad (14)$$

Q_{oil}^c and Q_{oil}^d are cumulative oil production of continuous and discontinuous polymer flooding process, respectively, t; P_{oil} is the oil price, \$/t; P_{ag}^c and P_{ag}^p are the prices of crosslinker and polymer for the anti-dilution slug, \$/t; P_p is the price of polymer for the polymer slug, \$/t; P_{lg}^c and P_{lg}^p are the prices of crosslinker and polymer for the long-acting gel slug, \$/t. M_{ag}^c and M_{ag}^p are the weight of crosslinker and polymer for the anti-dilution gel slug, \$/t; M_p is the weight of polymer for the polymer slug, t; M_{lg}^c and M_{lg}^p are the weight of the crosslinker and polymer for the long-acting gel slug, t. Table 2 shows the parameters used to calculate the NPV .

Table 2. The parameters used to calculate the NPV .

Parameters	Values
P_{ag}^p (\$/t)	2781
P_{ag}^c (\$/t)	2503
P_p (\$/t)	2781
P_{lg}^p (\$/t)	2781
P_{lg}^c (\$/t)	2503
P_{oil} (\$/t)	443

3.2. PSO–ICA Algorithm

A novel algorithm was developed by combining PSO and ICA algorithms to optimize various operational parameters for discontinuous polymer flooding processes. The establishment process is presented in Figure 3.

(1) Generation of initial empires

During the optimization process, a discontinuous polymer flooding scheme is considered as a country and has N_{var} of operational parameters needed to be optimized. Therefore, a country is defined as follows:

$$\vec{Country} = [p_1, p_1 \dots p_{N_{var}}] \quad (15)$$

Once the values of the operational parameters are given, the cost (the reciprocal of NPV) of each country C can be calculated by using CMG STARS:

$$c = f(p_1, p_2 \dots p_{N_{var}}) \tag{16}$$

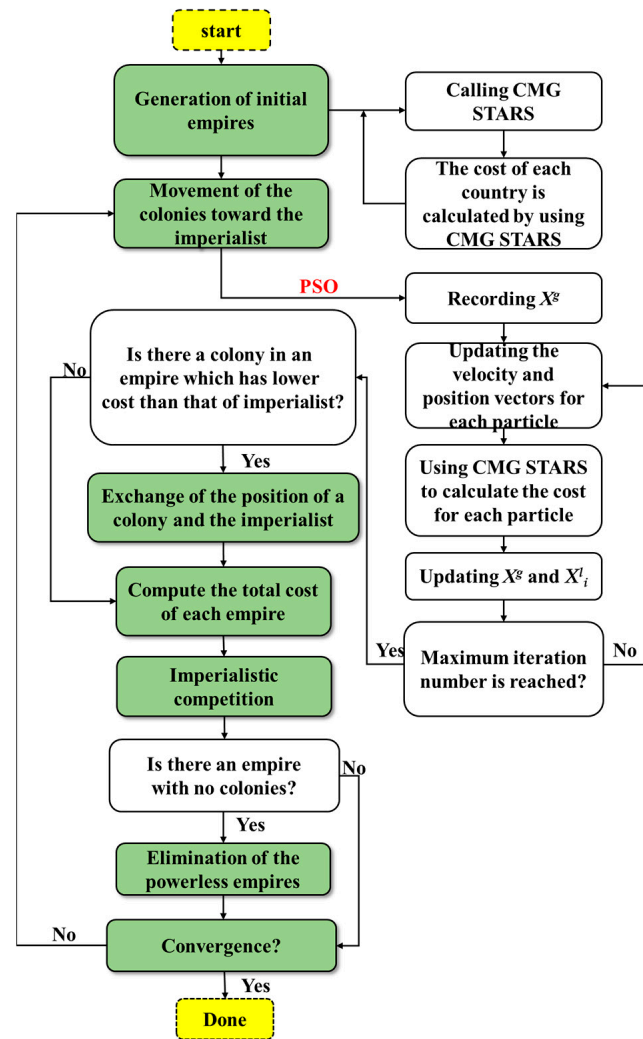


Figure 3. The establishment process of PSO-ICA algorithm.

To generate an initial empire, N_{pop} of countries is generated. Among the N_{pop} of countries, there are N_{imp} of imperialist and N_{col} of colonies. The relationship between N_{pop} , N_{imp} , and N_{col} satisfies the following equation:

$$N_{pop} = N_{imp} + N_{col} \tag{17}$$

The value of N_{col} of an empire depends on its power. The normalized power of each imperialist P_n is obtained by the following:

$$P_n = \left| \frac{C_n}{\sum_{i=1}^{N_{imp}} C_i} \right| \tag{18}$$

$$C_n = c_n - \max_i \{c_i\} \quad i = 1, 2, \dots, N_{imp} \tag{19}$$

where c_n is the cost of nth imperialist and C_n is the normalized cost of an imperialist. The initial number of colonies for each empire $N.C_n$ is as follows:

$$N.C_n = \text{round}\{P_n \cdot N_{\text{col}}\} \quad (20)$$

(2) Movement of the colonies toward the imperialist by PSO algorithm

In the traditional ICA, the movement of the colonies toward the imperialist is described by the following equation:

$$x \sim U(0, \beta \times d) \quad (21)$$

$$\theta \sim U(-\gamma, \gamma) \quad (22)$$

where x is the value of movement; d is the distance between the imperialist and colony; β is a number greater than unity; θ is a random number; γ is a parameter for the deviation from the original direction.

In this study, to enhance the search capability of the traditional ICA algorithm, PSO was introduced into ICA to replace the aforementioned method (Equations (23) and (24)). For the PSO algorithm, a group of particles is distributed as points in the space [43–45]. Each particle has the velocity and position vectors, which are defined by the following:

$$\vec{V}_i^t = [v_{i1}, v_{i2} \dots v_{iN}] \quad (23)$$

$$\vec{X}_i^t = [x_{i1}, x_{i2} \dots x_{iN}] \quad (24)$$

where x_{iN} means the n th operational parameters of discontinuous polymer flooding that need to be optimized at the time step t . A position vector represents a scheme of discontinuous polymer flooding.

For each particle, the NPV is calculated by using CMG STARS based on the position vector. If the NPV of a particle is higher than those of all the previous particles, the position vector of the particle is saved as the best position vector (X_i^1). If a particle has the highest NPV among all particles in that specific step, its position vector is saved in the global best position vector (X^g). The velocity and position vectors in each step are updated based on the following equations:

$$\vec{V}_i^{t+1} = \eta \vec{V}_i^t + \alpha_1 \gamma_1 (\vec{X}_i^1 - \vec{X}_i^t) + \alpha_2 \gamma_2 (\vec{X}^g - \vec{X}_i^t) \quad (25)$$

$$\vec{X}_i^{t+1} = \vec{X}_i^t + \vec{V}_i^{t+1} \quad (26)$$

where η is the inertia weight; γ_1 and γ_2 are variables in the range of [0, 1], respectively; α_1 and α_2 are the cognitive and the social factors, respectively. The aforementioned steps are repeated several times until the maximum iteration number is reached.

(3) Exchange of the position of a colony and the imperialist

After a colony is moved toward the imperialist, the values of the operational parameters are updated and have a higher NPV than these of the previous state. Then, the algorithm continues with the new values of the imperialist and the colonies.

(4) Total power of an empire

The total cost of the n th empire $T.C_n$ is defined as follows:

$$T.C_n = c(\text{imperialist}_n) + \omega \{c(\text{colonies}_n)\} \quad (27)$$

where ω is a positive number; imperialist_n and colonies_n are the total cost of the imperialist and colonies.

(5) Imperialistic competition

All the empires compete with each other based on their power. The empire with the largest power will possess the weakest colonies of the weakest empires.

(6) Elimination of the powerless empires

Because some empires are powerless, their colonies are possessed by other empires during the competition process. An empire will be eliminated when it loses all the colonies.

(7) Convergence

After the competition process, the powerful empire possesses all the colonies and the other empires are eliminated. The algorithm is finished.

4. Results

The developed PSO–ICA algorithm was first analyzed on benchmark functions and compared against ICA and PSO algorithms to evaluate its reliability. Then, the PSO–ICA algorithm was used to optimize the operational parameters of discontinuous polymer flooding to maximize the NPV.

4.1. Validation by Benchmark Functions

The developed PSO–ICA algorithm was analyzed on four benchmark functions. Details of these four functions are shown in Table 3.

Table 3. Description of the four benchmark functions.

Function Name	Function Equation	Dimensions	Definition Domain	Optimal Solution
F1	$Y = \sum_{i=1}^{10} \left x_i + \frac{1}{2} \right ^2$	10	[−100, 100]	0
F2	$Y = \sum_{i=1}^{10} (x_i^2 - 10 \cos(2\pi x_i)) + 100$	10	[−5.12, 5.12]	0
F3	$Y = \sum_{i=1}^{10} (-x_i \cdot \sin(\sqrt{ x_i }))$	10	[−500, 500]	−4190
F4	$Y = \sum_{i=1}^{10} x_i^2$	10	[−100, 100]	0

Figure 4 shows the analysis results of the PSO–ICA algorithm on four benchmark functions. The individual’s search history shows that the individual searches the main space of the four functions, indicating that the PSO–ICA algorithm has a strong search ability. In addition, the search history is concentrated around the optimal solution (red dot), which means that the PSO–ICA algorithm has a fast convergence speed. An individual’s trajectory shows that the solutions of the four functions have large fluctuations when the iteration number is small (the fluctuation range exceeds 34.15% of the space). However, with the increase in iteration number, the solutions of the four functions tend to be stable. The results proved that the PSO–ICA algorithm has a strong search ability in the function space and can quickly find the optimal solutions. It is noted that the solutions of F1 and F3 become stable and then fluctuate again, meaning that the algorithm jumps out of the locally optimal solution. In addition, Figure 4 shows that the average fitness and best fitness values quickly decrease with the increase in iteration numbers, reflecting that the algorithm has a high convergence speed. In addition, it can be seen from Table 4 that PSO–ICA algorithm has more accurate solutions and less iteration numbers for the four benchmark functions.

Table 4. Comparison of PSO–ICA with PSO and ICA on the four benchmark functions.

Algorithm	F1		F2		F3		F4	
	Solutions	Iteration Numbers	Solutions	Iteration Numbers	Solutions	Iteration Numbers	Solution	Iteration Numbers
ICA	10^{-1}	62	10^{-3}	147	−2221.74	150	2.5×10^{-144}	12
PSO	10^{-5}	265	17.81	>300	−4170.25	>300	0.000742	18
PSO–ICA	10^{-13}	3	10^{-14}	20	−4189.794	21	2.08×10^{-140}	10

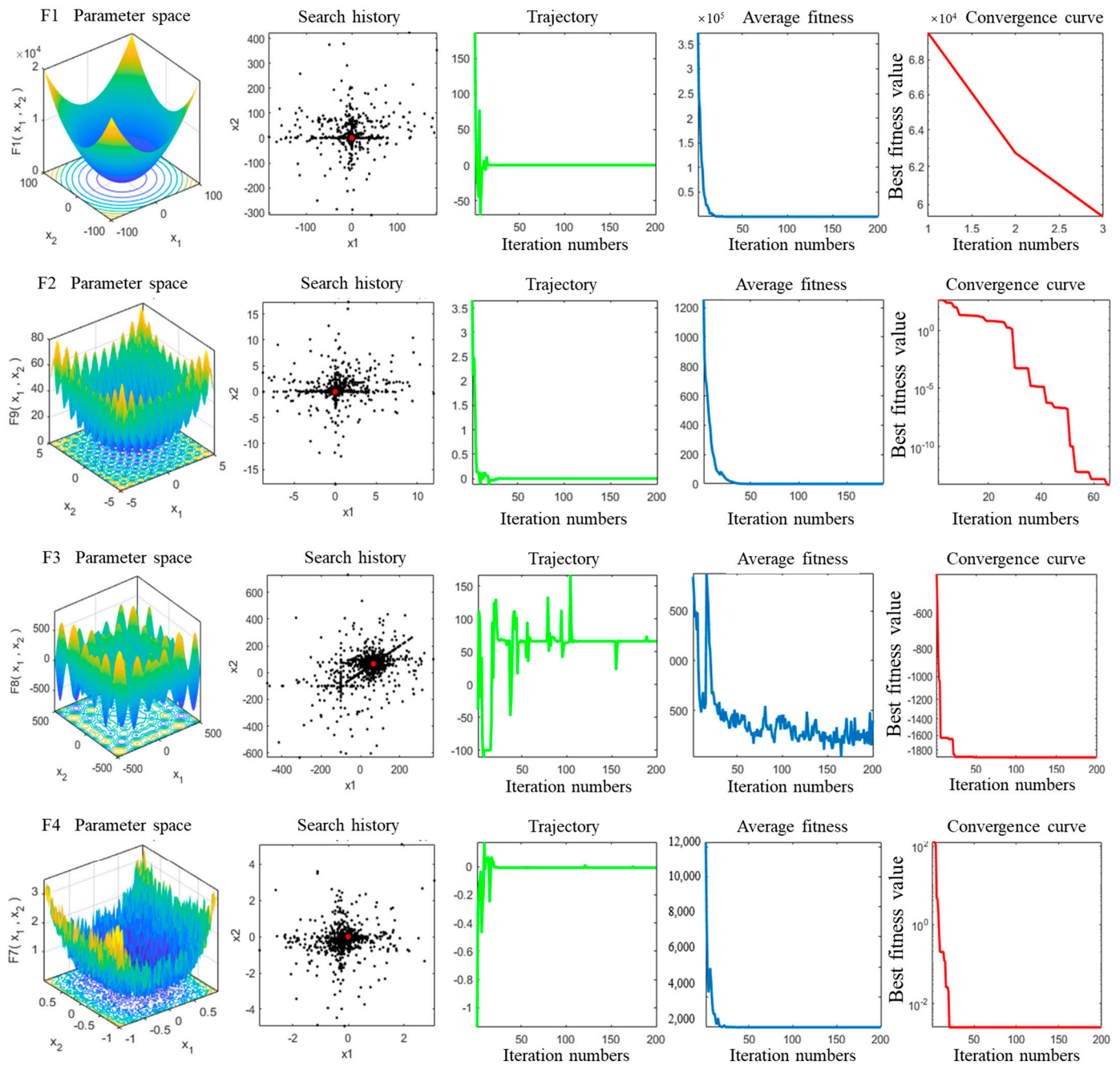


Figure 4. The analysis results of the PSO-ICA algorithm on the four benchmark functions.

Figure 5 provides a comparison of the convergence rate of the three algorithms. As shown in Figure 5, the convergence rate of the PSO-ICA is the fastest among all the three algorithms. Its better performance is attributed to the introduction of PSO into the ICA, which effectively enhances the search capability of the ICA algorithm and prevents the PSO-ICA from falling into the locally optimal solutions.

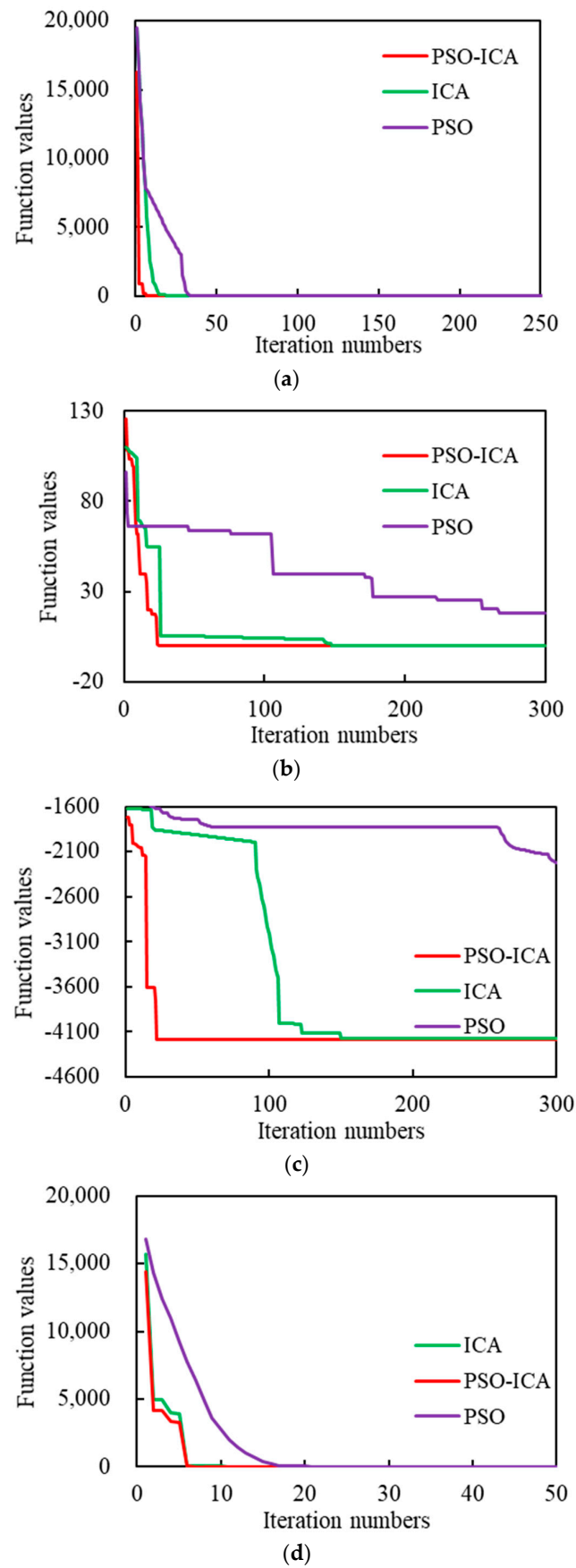


Figure 5. Comparisons of the convergence rate between PSO-ICA, PSO, and ICA on (a) F1, (b) F2, (c) F3, and (d) F4.

4.2. Optimization of Discontinuous Polymer Flooding by the PSO–ICA Algorithm

The PSO–ICA algorithm was used to find the optimal operational parameters of discontinuous polymer flooding. The parameter values used in the algorithm are determined by the sensitivity analysis and shown in Table 5.

Table 5. Parameters used in the PSO–ICA algorithm.

Parameters	Values
N_{pop}	10
N_{imp}	5
N_{col}	5
η	0.5
α_1, α_2	2
γ_1	0.8
γ_2	0.75
ω	0.1

Figure 6 shows the changes of the NPV with iteration numbers during the optimization process. It can be seen from Figure 6 that the NPV increases with the increase in iteration numbers. After 30 iterations, the optimal scheme achieved the highest NPV (7.49×10^8 \$).

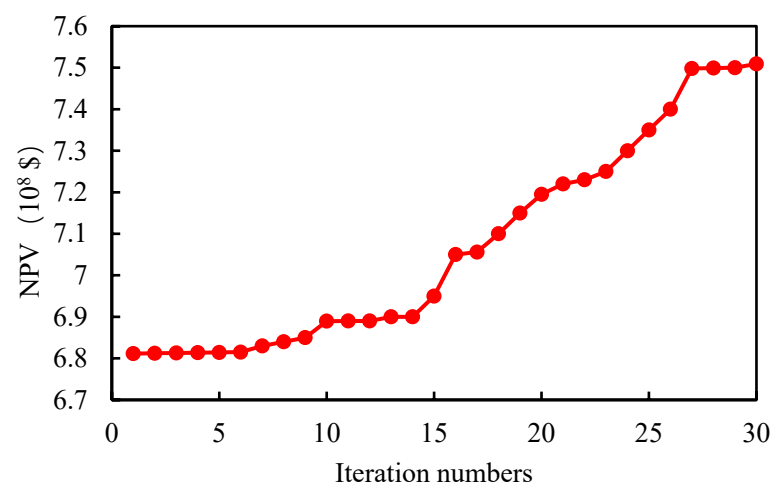


Figure 6. Changes of NPV with iteration numbers.

Figure 7 exhibits the optimization process of the operational parameters of Well P07. The values of the operational parameters are distributed in the entire range at the first iteration. However, after 30 iterations, they are concentrated in the optimal values. Table 6 gives the optimal operational parameters of the 12 injection wells. The results indicate that the PSO–ICA algorithm can be used to determine the optimal operational parameters of discontinuous polymer flooding processes which maximize the NPV.

Figure 8 shows a comparison of performance between the optimal schemes of discontinuous and continuous polymer flooding, indicating that the discontinuous polymer flooding scheme has a higher NPV, a lower water cut, a higher oil production rate, and a lower residual oil saturation. Specially, the NPV value of the optimal scheme of discontinuous polymer flooding reached 7.49×10^8 \$, which was an increase of 6% over that of the scheme of continuous polymer flooding. Therefore, discontinuous polymer flooding is an economical and effective method for enhancing oil recovery for offshore oilfields. The main reasons are that the injection of anti-dilution gel and long-acting gel slug effectively sealed the higher-permeability zones, increasing the sweep efficiency of polymer flooding (Figure 8), and the injection of polymer slug with a low concentration decreased the injection pressure and application cost of polymer flooding. In the future, more research

including selecting more reasonable parameters of the PSO-ICA algorithm to increase its optimization accuracy and convergence rate, comparing with other available optimization algorithms, and verifying the performance of the optimal scheme of discontinuous polymer flooding in the practical offshore oilfield will be required.

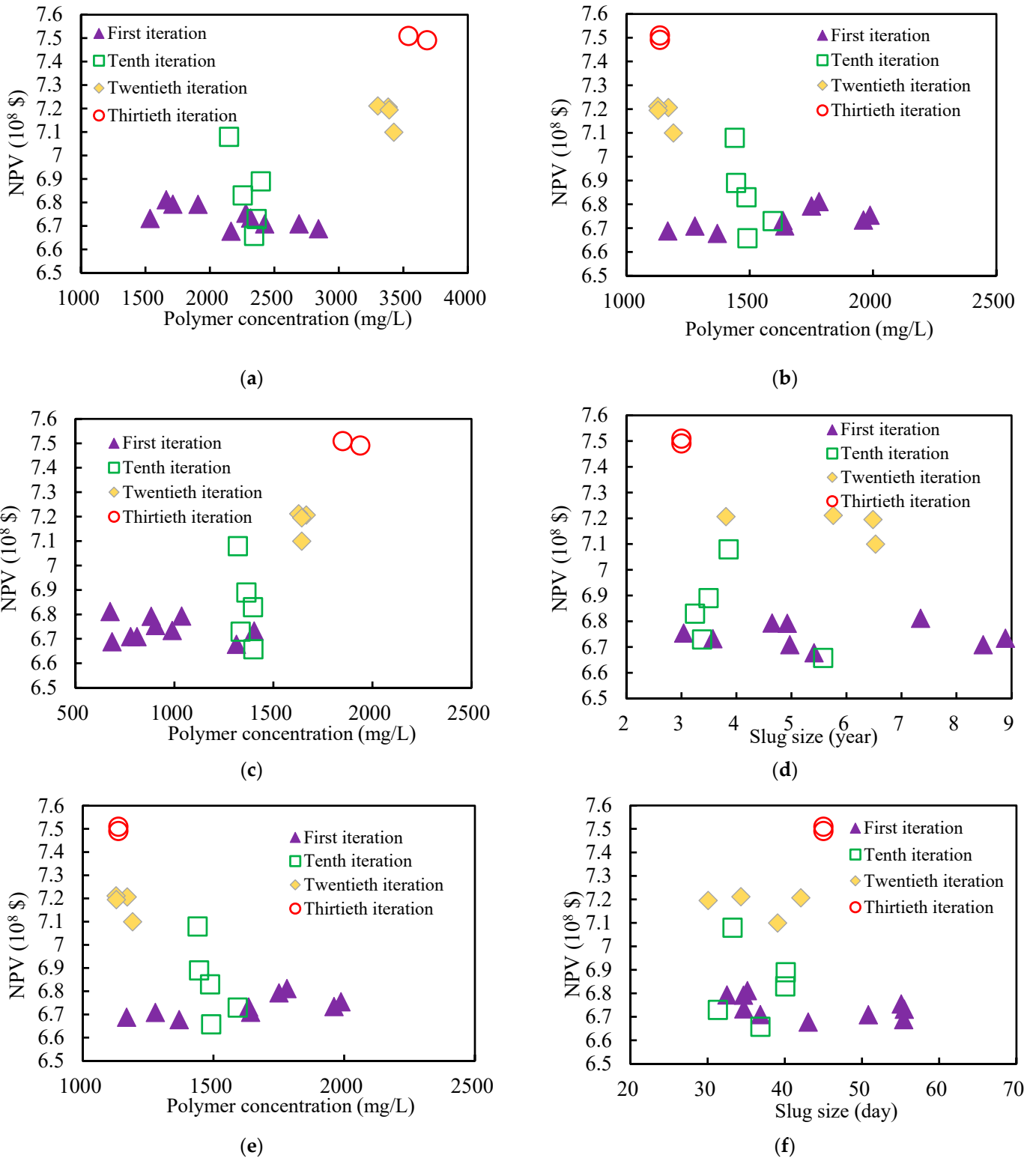


Figure 7. Cont.

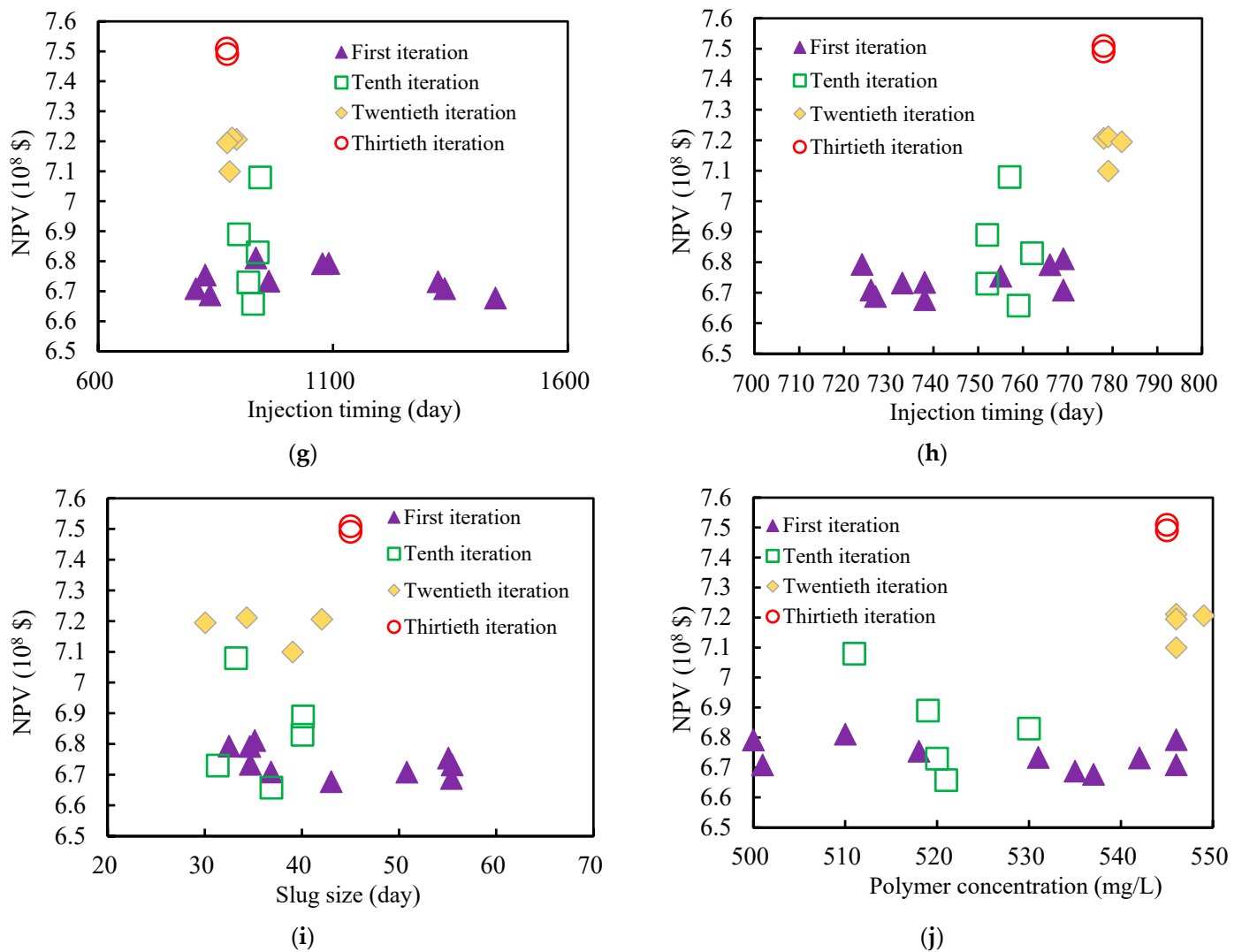


Figure 7. The optimization process of the operational parameters for well P07: (a) polymer concentration of anti-dilution gel slug, (b) polymer concentration of polymer slug, (c) polymer concentration of long-acting gel slug, (d) size of the anti-dilution gel slug, (e) size of polymer slug, (f) size of long-acting gel slug, (g) injection timing of long-acting gel slug, (h) injection timing of polymer slug with low concentrations, (i) size of polymer slug with low concentrations, and (j) polymer concentration of polymer slug with low concentrations.

Table 6. The optimal operational parameters of the 12 injection wells.

Well Name and Operational Parameters	Polymer Concentration of Anti-Dilution Gel Slug (mg/L)	Polymer Concentration of Polymer Slug (mg/L)	Polymer Concentration of Long-Acting Gel Slug (mg/L)	Size of the Anti-Dilution Gel Slug (day)	Size of Polymer Slug (year)	Size of Long-Acting Gel Slug (day)	Injection Timing of Long-Acting Gel Slug (day)	Polymer Concentration of Polymer Slug with Low Concentrations (mg/L)	Size of Polymer Slug with Low Concentrations (day)	Injection Timing of Polymer Slug with Low Concentrations (day)	Polymer Concentration of Anti-Dilution Gel Slug (mg/L)	Polymer Concentration of Polymer Slug (mg/L)
P07	3684	1136	1939	28	3	45	875	545	49	778	3684	1136
P09	1505	1200	1768	21	5	25	821	550	45	722	1505	1200
P11	3035	1407	1872	40	6	60	1429	564	55	1330	3035	1407
P16	2293	800	1735	39	3	29	421	588	52	336	2293	800
P18	1864	1458	1927	20	4	47	1183	603	41	1100	1864	1458
P19	3921	992	1888	39	3	59	1171	618	53	1079	3921	992
P21	3056	1337	1747	41	3	20	900	629	42	807	3056	1337
P23	2759	864	1554	32	4	48	1032	634	58	940	2759	864
I14	2821	1566	1500	38	3	52	1118	662	41	1022	2821	1566
I26	3201	1183	1735	37	4	35	2108	677	41	2022	3201	1183

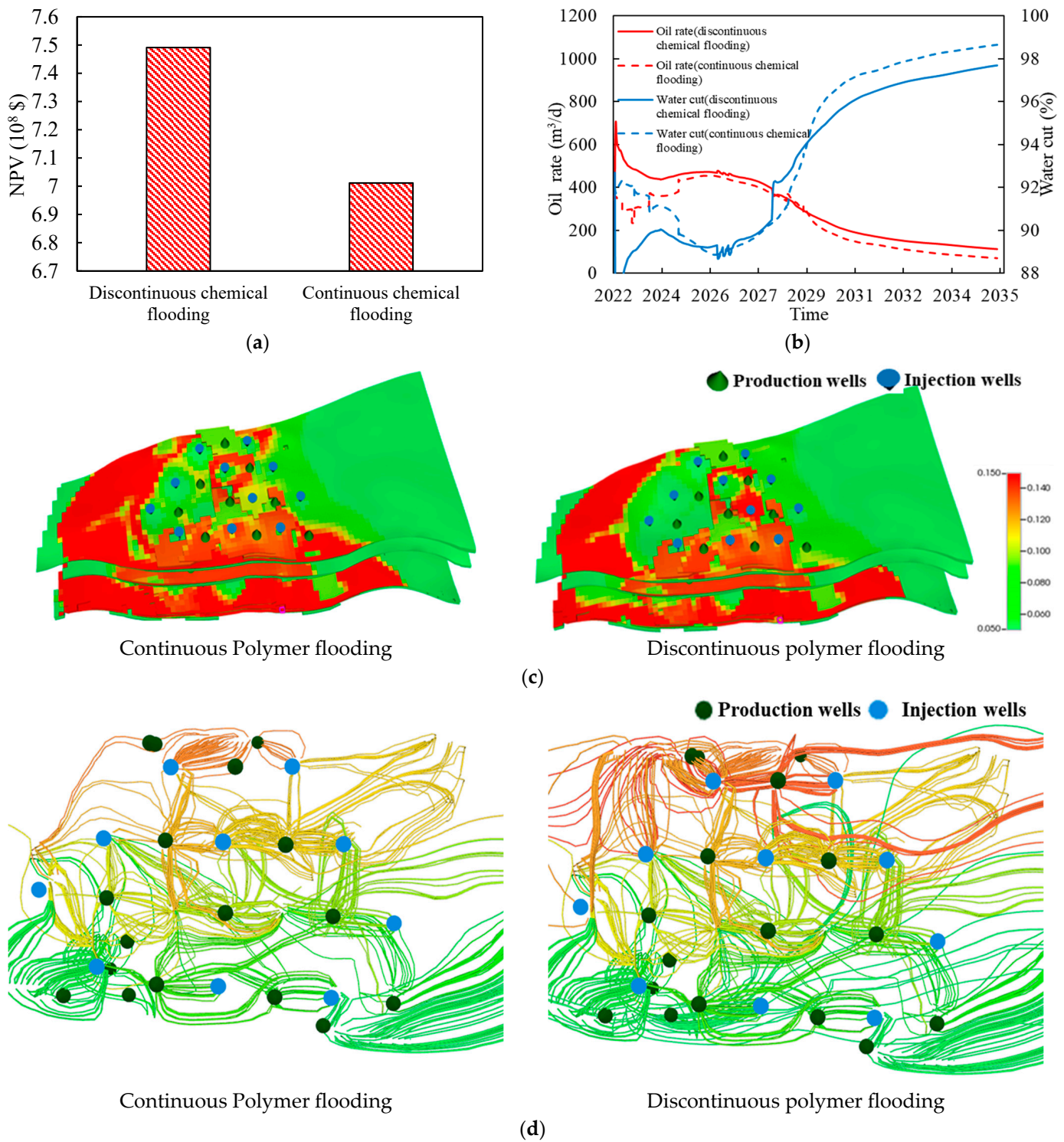


Figure 8. A comparison of performance between the optimal scheme of discontinuous and continuous polymer flooding: (a) NPV, (b) oil production rate and water cut, (c) residual oil saturation distribution, and (d) chemical streamlines distribution.

5. Conclusions

- (1) The introduction of PSO into ICA effectively enhances the search capability of the ICA and prevents PSO–ICA from falling into local optimum. Therefore, PSO–ICA has lower iteration numbers, higher optimization accuracy, and faster convergence rate than these of PSO and ICA.

- (2) The developed PSO–ICA algorithm provides an effective method for optimizing the operational parameters of discontinuous polymer flooding processes by maximizing the NPV value. More applications are needed to further verify the accuracy of the PSO–ICA algorithm.
- (3) Compared to continuous polymer flooding, discontinuous polymer flooding has a higher NPV, a higher oil production rate, a lower water cut, and a lower residual oil saturation. The injection of an anti-dilution gel slug, long-acting gel slug, and polymer slug with a low concentration effectively sealed the higher-permeability zones, improved the sweep efficiency of polymer flooding, and decreased the injection pressure and application cost.
- (4) The NPV value of the optimal scheme of discontinuous polymer flooding reached 7.49×10^8 \$, which is an increase of 6% over that of the scheme of continuous polymer flooding. Discontinuous polymer flooding is an economical and effective method for enhancing oil recovery for offshore oilfields.

Author Contributions: Conceptualization, J.Z.; Methodology, E.T.; Validation, L.L.; Investigation, B.Z.; Resources, Y.J.; Writing—original draft, A.X.; Writing—review & editing, X.S.; Supervision, X.S. All authors have read and agreed to the published version of the manuscript.

Funding: This research was funded by the Key Technologies R&D Program of CNOOC (KJGG2021-0504) and CNOOC Research Institute Limited’s research and development project (No. CCL2022RCPS0553RSN).

Data Availability Statement: The original contributions presented in the study are included in the article, further inquiries can be directed to the corresponding authors.

Conflicts of Interest: Authors Engao Tang, Jian Zhang, Yi Jin and Lezhong Li were employed by the company CNOOC Research Institute Limited. The remaining authors declare that the research was conducted in the absence of any commercial or financial relationships that could be construed as a potential conflict of interest.

References

1. Pope, G.A. Recent developments and remaining challenges of enhanced oil recovery. *J. Pet. Technol.* **2011**, *63*, 65–68. [[CrossRef](#)]
2. Sheng, J.J.; Leonhardt, B.; Azri, N. Status of polymer-flooding technology. *J. Can. Pet. Technol.* **2015**, *54*, 116–126. [[CrossRef](#)]
3. Wang, D.; Cheng, J.; Xia, H.; Li, Q.; Shi, J.P. Viscous-Elastic fluids can mobilize oil remaining after Water-Flood by force parallel to the Oil-Water interface. In Proceedings of the SPE Asia Pacific Improved Oil Recovery Conference, Kuala Lumpur, Malaysia, 8–9 October 2001.
4. Wei, B.; Romero-Zerón, L.; Rodrigue, D. Oil displacement mechanisms of viscoelastic polymers in enhanced oil recovery (EOR): A review. *J. Pet. Explor. Prod. Technol.* **2014**, *4*, 113–121. [[CrossRef](#)]
5. Zhang, K.; Choi, H.J.; Jang, C.H. Turbulent drag reduction characteristics of poly (acrylamide-co-acrylic acid) in a rotating disk apparatus. *Colloid. Polym. Sci.* **2011**, *289*, 1821–1827. [[CrossRef](#)]
6. Meter, D.M.; Bird, R.B. Tube flow of non-Newtonian polymer solutions: PART I. Laminar flow and rheological models. *AIChE J.* **1964**, *10*, 878–881. [[CrossRef](#)]
7. Dovan, H.T.; Hutchins, R.D.; Terzian, G.A. Dos cuadradas offshore polymer flood. In Proceedings of the SPE California Regional Meeting, Ventura, CA, USA, 4–6 April 1990.
8. Pan, G.M.; Zhang, L.; Huang, J.; Li, H.; Qu, J.F. Twelve years field applications of offshore heavy oil polymer flooding from continuous injection to alternate injection of polymer-water. In Proceedings of the Offshore Technology Conference Asia, Kuala Lumpur, Malaysia, 2–6 November 2020.
9. Rathinasamy, M.; Chandramouli, S.; Phanindra, K.B.V.N. *Estimation of Reservoir Storage Using Artificial Neural Network*; Springer: Singapore, 2018; pp. 57–63.
10. Liu, B.; Bai, B.; Li, Y. Research on preformed gel grains for water shutoff and profile control. *Oil Drill. Prod. Technol.* **1999**, *21*, 65–68. (In Chinese)
11. Bai, B.; Li, Y.; Liu, X. New development of water shutoff and profile control in oilfields in China. *Oil Drill. Prod. Technol.* **1999**, *20*, 64–68. (In Chinese)
12. Bai, B.; Li, L.X.; Liu, Y.Z.; Liu, H.; Wang, Z.G.; You, C.M. Preformed particle gel for conformance control: Factors affecting its properties and applications. *SPE Reservoir Eval. Eng.* **2007**, *10*, 415–422. (In Chinese) [[CrossRef](#)]
13. Bai, B.J.; Huang, F.S.; Liu, Y.Z.; Seright, R.S.; Wang, Y.F. Case study on preformed particle gel for in-depth fluid diversion. In Proceedings of the SPE Symposium on Improved Oil Recovery, Tulsa, OK, USA, 20–23 April 2008.

14. Tongwa, P.; Nygaard, R.; Bai, B. Evaluation of a nanocomposite hydrogel for water shut-off in enhanced oil recovery applications: Design, synthesis, and characterization. *J. Appl. Polym. Sci.* **2013**, *128*, 787–794. [[CrossRef](#)]
15. Tongwa, P.; Nygaard, R.; Bai, B.; Blue, A. Evaluation of potential fracture-sealing materials for remediating CO₂ leakage pathways during CO₂ sequestration. *Int. J. Greenhouse Gas. Control.* **2013**, *18*, 128–138. [[CrossRef](#)]
16. Tongwa, P.; Baojun, B. A more superior preformed particle gel with potential application for conformance control in mature oilfields. *J. Pet. Explor. Prod. Technol.* **2015**, *5*, 201–210. [[CrossRef](#)]
17. Claridge, E.L. A method for designing graded viscosity banks. *Soc. Pet. Eng. J.* **1978**, *18*, 315–324. [[CrossRef](#)]
18. Zhang, J. Study on discontinuous chemical flooding model of offshore high water cut oilfield. *Zhongguo Haishang Youqi* **2023**, *35*, 70–77. (In Chinese)
19. Standnes, D.C.; Skjevraak, I. Literature review of implemented polymer field projects. *J. Pet. Sci. Eng.* **2014**, *122*, 761–775. [[CrossRef](#)]
20. Seright, R.S. How much polymer should be injected during a polymer flood? Review of previous and current practices. *SPE J.* **2017**, *22*, 1–18. [[CrossRef](#)]
21. Bagheri, A.; Razeghi, H.R.; Amiri, G.G. Detection and estimation of damage in structures using imperialist competitive algorithm. *Noise Control* **2012**, *19*, 405–419. [[CrossRef](#)]
22. Beghi, A.; Cecchinato, L.; Cosi, G.; Rampazzo, M. A PSO-based algorithm for optimal multiple chiller systems operation. *Appl. Therm. Eng.* **2012**, *32*, 31–40. [[CrossRef](#)]
23. Shao, W.; Cui, Z.; Cheng, L. Multi-objective optimization of cooling air distributions of grate cooler with different clinker particles diameters and air chambers by genetic algorithm. *Appl. Therm. Eng.* **2017**, *111*, 77–86. [[CrossRef](#)]
24. Yang, M.D.; Lin, M.D.; Lin, Y.H.; Tsai, K.T. Multiobjective optimization design of green building envelope material using a non-dominated sorting genetic algorithm. *Appl. Therm. Eng.* **2017**, *111*, 1255–1264. [[CrossRef](#)]
25. Sayyafzadeh, M.; Keshavarz, A. Optimisation of gas mixture injection for enhanced coalbed methane recovery using a parallel genetic algorithm. *J. Nat. Gas. Sci. Eng.* **2016**, *33*, 942–953. [[CrossRef](#)]
26. Eshraghi, S.E.; Rasaei, M.R.; Zendejboudi, S. Optimization of miscible CO₂ EOR and storage using heuristic methods combined with capacitance/resistance and Gentil fractional flow models. *Nat. Gas. Sci. Eng.* **2016**, *32*, 304–318. [[CrossRef](#)]
27. Ahmadi, M.A.; Soleimani, R.; Lee, M.; Kashiwao, T.; Bahadori, A. Determination of oil well production performance using artificial neural network (ANN) linked to the particle swarm optimization (PSO) tool. *Petroleum* **2015**, *1*, 118–132. [[CrossRef](#)]
28. Dossary, M.A.A.; Nasrabadi, H. Well placement optimization using imperialist competitive algorithm. *J. Pet. Sci. Eng.* **2016**, *147*, 237–248. [[CrossRef](#)]
29. Abd-Elazim, S.A.E. Power system stability enhancement via bacteria foraging optimization algorithm. *Arabian J. Sci. Eng.* **2013**, *38*, 599–611. [[CrossRef](#)]
30. Abd-Elazim, S.A.E. Imperialist competitive algorithm for optimal statcom design in a multimachine power system. *Int. J. Elec. Power.* **2016**, *76*, 136–146. [[CrossRef](#)]
31. Moradifar, A.; Akbari, F.A.; Gorgani, F.K. Comprehensive identification of multiple harmonic sources using fuzzy logic and adjusted probabilistic neural network. *Neural Comput. Appl.* **2017**, *31*, 543–556. [[CrossRef](#)]
32. Mortazavi, A.; Khamseh, A.A.; Naderi, B. A novel chaotic imperialist competitive algorithm for production and air transportation scheduling problems. *Neural Comput. Appl.* **2015**, *26*, 1709–1723. [[CrossRef](#)]
33. Zandieh, M.; Khatami, A.; Rahmati, S.H.A. Flexible job shop scheduling under condition-based maintenance: Improved version of imperialist competitive algorithm. *Appl. Soft Comput.* **2017**, *58*, 449–464. [[CrossRef](#)]
34. Mikaeil, R.; Haghshenas, S.S.; Haghshenas, S.S.; Ataei, M. Performance prediction of circular saw machine using imperialist competitive algorithm and fuzzy clustering technique. *Neural Comput. Appl.* **2018**, *29*, 283–292. [[CrossRef](#)]
35. Hosseini, S.; Khaled, A.A.; Vadlamani, S. Hybrid imperialist competitive algorithm, variable neighborhood search, and simulated annealing for dynamic facility layout problem. *Neural Comput. Appl.* **2014**, *25*, 1871–1885. [[CrossRef](#)]
36. Bahrami, H.; Faez, K.; Abdechiri, M. Imperialist competitive algorithm using chaos theory for optimization (CICA). In Proceedings of the International Conference on Computer Modelling and Simulation, Cambridge, UK, 24–26 March 2010.
37. Abdechiri, M.; Faez, K.; Bahrami, H. Neural network learning based on chaotic imperialist competitive algorithm. In Proceedings of the 2010 2nd International Workshop on Intelligent Systems and Applications, Wuhan, China, 7 June 2010.
38. Abdechiri, M.; Faez, K.; Bahrami, H. Adaptive imperialist competitive algorithm (AICA). In Proceedings of the 9th IEEE International Conference on Cognitive Informatics (ICCI'10), Beijing, China, 7–9 July 2010.
39. Khaled, A.A.; Hosseini, S. Fuzzy adaptive imperialist competitive algorithm for global optimization. *Neural Comput. Appl.* **2015**, *26*, 813–825. [[CrossRef](#)]
40. Gao, S.L.; Chen, Y.; Wang, X.; Li, S.Q.; Yan, S.G.; Hou, B.F. Research on dynamic performance of anti-polymer adsorbent in Henan oilfield. *Dangdai Huagong* **2021**, *50*, 2170–2175. (In Chinese)
41. Zhang, P.; Tan, X.; Yang, R.; Yang, R.F.; Zheng, W.; Zhang, X.L.; Xie, H.J.; Sun, X.F. Numerical Simulations of Nitrogen Foam and Gel-Assisted Steam Flooding for Offshore Heavy Oil Reservoirs. *J. Porous Media* **2023**, *26*, 17–32. [[CrossRef](#)]
42. Zandvliet, M.J.; Handels, M.; Van, E.G.M.; Brouwer, D.R.; Jansen, J.D. Adjoint-based well-placement optimization under production constraints. *SPE J.* **2008**, *13*, 392–399. [[CrossRef](#)]
43. Askarzadeh, A. Comparison of particle swarm optimization and other metaheuristics on electricity demand estimation: A case study of Iran. *Energy* **2014**, *72*, 484–491. [[CrossRef](#)]

44. Ahirwal, M.K.; Kumar, A. Singh G K. Analysis and testing of PSO variants through application in EEG/ERP adaptive filtering approach. *Open Biomed. Eng. Lett.* **2012**, *2*, 186–197. [[CrossRef](#)]
45. Atif, E.A.; Ibrahim, M.A.; Shehata, O.M. Performance evaluation of PSO-PID and PSO-FLC for continuum robot's developed modeling and control. *Sci. Rep.* **2024**, *14*, 733.

Disclaimer/Publisher's Note: The statements, opinions and data contained in all publications are solely those of the individual author(s) and contributor(s) and not of MDPI and/or the editor(s). MDPI and/or the editor(s) disclaim responsibility for any injury to people or property resulting from any ideas, methods, instructions or products referred to in the content.